

Thermal and mechanical evaluation of the thermal barrier layers coated by spray dried granules

Ju Hyoung Cho^a, Tae Woo Kim^a, Yeon Gil Jung^b and Kee Sung Lee^{a,*}

^aSchool of Mechanical and Automotive Engineering, Kookmin University, 861-1 Chongnungdong, Songbukgu, Seoul 136-702, Korea

^bSchool of Nano & Advanced Materials Engineering, Changwon University, 9 Sarimdong, Changwon, Kyungnam 641-773, Korea

In this study yttrium stabilized zirconia (YSZ) spray dried granules are produced and applied for thermal barrier coatings in gas turbine applications. The morphologies of the spray dried granules are varied by the control of the solvent type, binder/dispersant content and process parameters during spray drying. The feed rate depends on the morphologies of the granules. The spray dried granules are deposited over a NiCrCoAlY bond coat by an air plasma spray coating apparatus for the thermal barrier coatings. We evaluated the thermal tolerance of the thermal barrier layers by thermal annealing tests and hardness tests after the thermal annealing tests. As a result, the thermal barrier coating using pre-heat treated spherical powder gave advantages in thermal and mechanical resistances after the thermal annealing test.

Key words: Thermal barrier coating, Spray drying, Thermal and mechanical property.

Introduction

Recently, a high energy efficiency gas turbine system working at high temperature is strongly demanded to save energy and protect the environment. In such a system ceramic thermal barrier coatings have been widely used as a method to increase the energy efficiency of the gas turbine system because they can increase the operational temperature of the system without sacrificing subsurface metallic materials. Advanced gas turbine systems such as the G and H series choose ceramic thermal barrier coatings on the hot gas sections under critical loading conditions. Indeed, the advantage of a ceramic thermal barrier coating includes a potential increase in efficiency and power density [1-3]. Increased efficiency is closely related with savings of fuel consumption and reduction of the maintenance cost of cooling. Thermal barrier coatings consist of a thermal insulation ceramic top layer on an intermediate oxidation resistant bondcoat layer. Yttrium stabilized zirconia (YSZ) ceramics are the most widely used materials for thermal barrier coatings in advanced gas turbine systems owing to their low thermal conductivity, relatively high thermal expansion coefficient, comparable to the metallic substrate or bond coat, and high mechanical strength [4-5].

Plasma spraying in air, low pressure, or vacuum is increasingly used to make thermal barrier coatings for

advanced gas turbines. In this plasma spray technology, the feedstock powder is fed, melted in the plasma-enhanced flame and rapidly accelerated towards the substrate mechanically and finally solidifies. Thermal barrier coatings are developed by successive build-up of these splats. Metallic and ceramic feedstock powders with a 10-100 μm size are widely used in an air plasma spray (APS) system to create coatings with defined characteristics [6-8]. The feedstock powders are usually fabricated by a spray drying process [9-11]. Spray drying is a process by which a fluid feed material is transformed into a dried powder by spraying the feed into a hot chamber using a rotating atomizer. It is known that spray powders with a high porosity (10-20%) offer an advantage in their application in TBCs [9]. The microstructures of TBC layers are determined by the feedstock powders as well as the spraying conditions. In particular, the size, shape and density of the powders are critical in the coating microstructure and the most important parameters for the quality of the coating layer.

The thermal resistance of TBCs is closely related with the microstructure of the ceramic topcoat layer [11, 12]. Since the TBCs experience severe thermomechanical cycling in the gas turbine application, it is especially important to design TBCs with high durability and longer lifetime. Indeed, Zhu and Miller [13-15] showed that ceramic coating failure under severe thermal cycling conditions is closely related to coating surface cracking, microspallation and accelerated crack growth. They investigate the mechanisms of crack propagation and of coating failure under complex low cycle fatigue and high cycle fatigue condition. Evans and coworker [16-17] explained the TGO (thermal grown oxide) layer

*Corresponding author:
Tel : +82-2-910-4834
Fax: +82-2-910-4839
E-mail: keeslee@kookmin.ac.kr

undergoes displacement instability when the coating system is subject to thermal cycling. The downward displacements induce normal strains that cause cracks to form, extend laterally and, eventually coalesce to failure by buckling. The thermal resistances and failure mechanisms are closely related to the microstructure of the ceramic topcoat, which is in turn influenced by the ceramic powder morphology.

Therefore, in the present study, we are mainly concerned with the morphology of the spray dried granules to produce thermal resistant TBC layers. We prepared three sets of different powder morphologies, deformed/partially spherical/spherical powders using a spray drying process. We have evaluated the feed rate of the fabricated powders, and the thermal/mechanical properties of the TBC layers, which have been deposited by the three-typed spray dried granules using an air plasma spray (APS) apparatus. As a result, the thermal barrier coating using spherical powder gave advantages in thermal and mechanical tolerances after the thermal annealing test.

Experimental Procedure

The starting materials for the synthesis of feedstock powders using a co-precipitation method were a zirconium oxy-chloride ($ZrOCl_2 \cdot 8H_2O$) solution, doped with yttrium nitrate, $Y(NO_3)_3 \cdot 6H_2O$. The mixed solution was neutralized with an NH_3 solution to form a precipitate. The reaction mixture was stirred using a magnetic stirrer for 30 minutes, filtered, washed with deionized water and dried for 1 day and then calcined at $1000^\circ C$ for 2 h. The mixtures from these calcined cakes containing 8 wt% Y_2O_3 doped ZrO_2 , were crushed and sieved into a powder mixture. The mixture was dispersed into slurry with an organic solvent, binders, plasticizer as feedstock for spray drying. The powders were mixed as slurry with distilled water or alcohol for 24 h in a ball mill using ZrO_2 balls. The organic binder and dispersant as shown in Table 1 were added during ball milling. A constant inlet temperature, $170-210^\circ C$, and outlet temperature, $70-110^\circ C$, were maintained in each set of spray drying by checking with a thermocouple during the process. The atomizer speed was controlled from 6,000-10,000 rpm to control the size of the granules. The solid loading was 45-60 wt% for each batch of the slurry and a constant feeding of the slurry, 10 kg/h, was maintained during feeding into the hot chamber. The experimental procedure for the fabrication of granules used in the APS coating is shown in Fig. 1(a). Three conditions of agglomerates were prepared using spray drying instrument (Fine Tech. Incheon, Korea), deformed/

partially spherical/spherical powders as shown in Fig. 2. All through the paper, deformed granules synthesized from a water-based solution, partially spherical granules and relatively spherical granules from alcohol-based solutions are designated by YZ-W, YZ-AH and YZ-AS, respectively.

Heat treatments of the spray dried granules have been conducted to enhance the feeding and their mechanical properties. The powders were heated in an atmosphere at $1250^\circ C$ for 10 minutes after removing the organic additives in the temperature range of $600-800^\circ C$. Powder

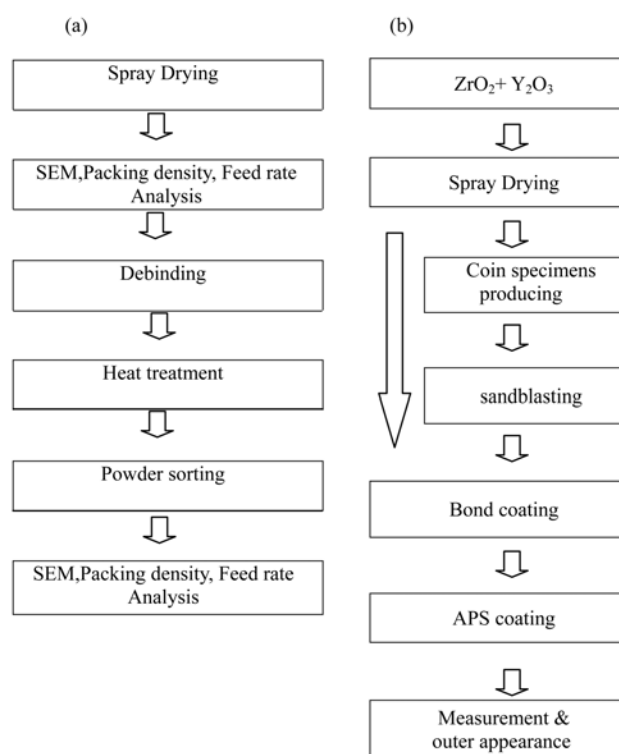


Fig. 1. Experimental procedures for the fabrication of (a) spray dried granules and (b) TBC layers.

Table 1. Types of solvents and organic additive materials used in the spray drying process

	Solvent	Binder	Disperser
YZ-W	Water	PVA 205	LU-6418
YZ-AH	Alcohol	PVB	PEG
YZ-AS	Alcohol	PVB	-

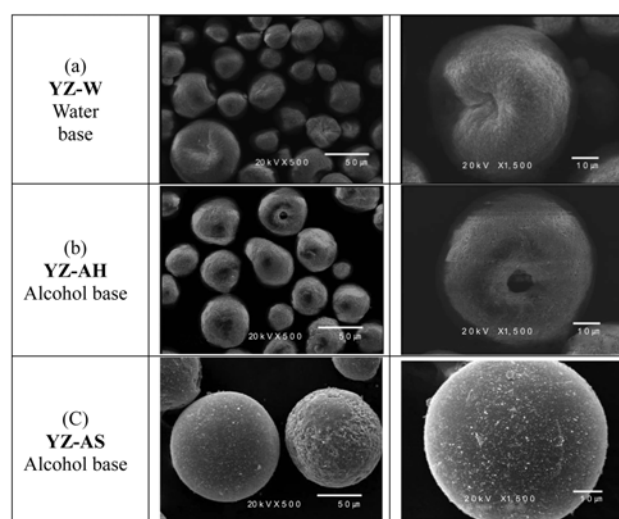


Fig. 2. SEM micrographs of spray dried granules; (a) YZ-W, (b) YZ-AH, and (c) YZ-AS.

Table 2. The results of classification by screening of spray dried granules produced from (a) a water-based solution (YZ-W) and (b) an alcohol-based solution (YZ-AH and YZ-AS)

(a)					
	~ -38 μm	+38 ~ -75 μm	+75 ~ -106 μm	+106 ~ -125 μm	+125 μm ~
Water base	12.8 (wt%)	81.5 (wt%)	4.1 (wt%)	1.4 (wt%)	0.2 (wt%)
(YZ-W)	11.9 (vol.%)	76.27 (vol.%)	6.78 (vol.%)	4.2 (vol.%)	0.85 (vol.%)
(b)					
	~ -38 μm	+38 ~ -75 μm	+75 ~ -106 μm	+106 ~ -125 μm	+125 μm
Alcohol base	10.8 (wt%)	83.3 (wt%)	4.6 (wt%)	0.2 (wt%)	1.1 (wt%)
(YZ-AH and YZ-AS)	11.9 (vol.%)	76.3 (vol.%)	6.8 (vol.%)	4.2 (vol.%)	0.85 (vol.%)

classifications have been conducted using an auto-sieving machine with a stack of sieves, 38, 45, 75, 106 and 125 μm , to classify the powder mixtures into constant ranges of sizes of granules. The detailed results from the classification of the granules by screening are summarized in Table 2.

The filling density and feed rate was measured to evaluate the flowability of the spray dried granules using a self-made laboratory-scale experimental unit. The spray dried powders were freely flowed into a container with a volume of approximately 100 cm^3 and a diameter to height ratio of 1. Then the filling density was calculated from the mass of the powder divided by the confined volume of the container. For feed rate measurements, the mass of a known volume of the powder was determined after allowing it to fall freely into a stationary container and then the falling time measured under specified conditions. The mass of the powder divided by the falling time after the test gives its feed rate by Eq. (1):

$$\text{Feed rate} = \{M_{\text{flowed}} - M_{\text{unflowed}}\} / \text{time} \quad (1)$$

where M_{flowed} is the mass of the flowing powder, and M_{unflowed} is the mass of the powder adhered to the walls of measuring instrument.

Plasma spraying was carried out using a 9 MB plasma gun (Sulzer-Metco, Switzerland). A nickel-based superalloy (GTD-111, General Electric Co., USA) as a substrate. The procedure for the fabrication of TBC layers is shown in Fig. 1(b). Flat rectangular test samples were machined test samples were machined from fully heat-treated GTD-111 turbine blade using an electro-discharge machining process. Prior to spraying, the substrate plates with the dimension of 25 mm diameter \times 2 mm thickness were ground and sand-blasted with abrasives. The same APS apparatus was applied to deposit a bond coat with a thickness of $d = 250 \mu\text{m}$ onto the substrates, using powdered Co-Ni-Cr-Al-Y alloy (AMDRY 263, Sulzer Metco, Switzerland), and then a top coat with a constant thickness of $d = 600\text{-}700 \mu\text{m}$ was air-plasma sprayed onto the bond coat, using powdered zirconia (ZrO_2) containing 8 wt% of yttria (Y_2O_3) developed in this study. The power of the apparatus and coating time was adjusted, in the range of 500-600 A and 80-100 V, to obtain constant thickness of TBC using the three granules, YZ-W, YZ-AH, YZ-AS.

The phases of the spray dried granules were qualitatively analyzed using an X-ray diffractometer (XRD, D/Max2000-Ultima Plus, Rigaku). The analyses were performed and compared to the feed materials produced from either the water-based batch or the organic solvent-based batches. Other analyses were performed and compared with feed materials without heat treatment and with granules heat treated at 1250 $^\circ\text{C}$ for 1h and 1350 $^\circ\text{C}$ for 1h, respectively.

The powder morphologies and the microstructures of the TBCs were investigated using a scanning electron microscope (SEM, XL30 Philips) or FE-SEM (JSM 7401F JEOL). A powder sample was embedded with a fluid epoxy resin, polished with a 1 mm diamond suspension on a cloth and observed using SEM.

Thermal annealing tests under a simulating operation temperature in the gas turbine application were conducted using high temperature furnace. The temperature was raised to 1210 $^\circ\text{C}$ at a rate of 1 $^\circ\text{C}\cdot\text{minute}^{-1}$ and held at the maximum temperature for a constant time, and then cooled down at the same rate. The thickness of the topcoat, bondcoat and TGO were checked by optical and scanning electron microscopes. Microstructures were examined before and after the thermal annealing tests. Microhardness measurements were made by Vickers indentations. The tests were conducted before and after the thermal annealing tests. Load of $P = 10 \text{ N}$ was applied on the sectioned surfaces of TBC. The hardness of the TBC material was calculated from Eq. (2) :

$$H_v = \frac{P}{2 \left(\frac{d}{2} \right)^2} \quad (2)$$

where d is the indentation diagonal length.

Results and Discussion

Fig. 2 shows the granules with different powder morphologies which vary by solvent type, binder/dispersant content and process parameters during the spray drying process. Fig. 2(a) shows deformed granules synthesized in a water-based solution (YZ-W), (b) partially spherical granules in an alcohol-based solution (YZ-AH) and relatively spherical granules in an alcohol-based solution (YZ-AS), respectively. The sprayed dried granules have been applied

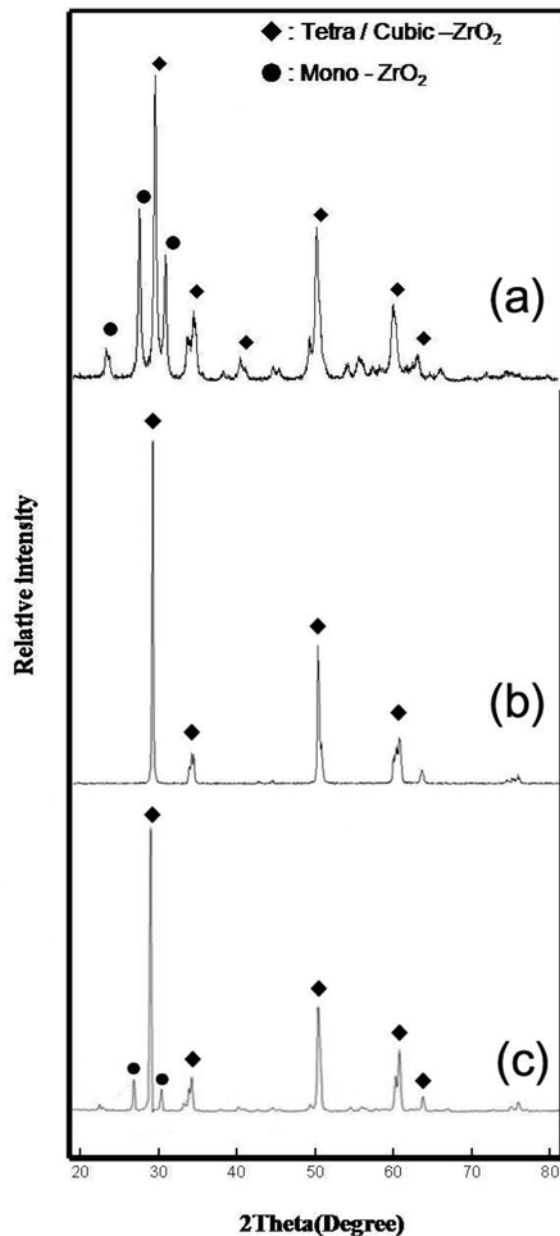


Fig. 3. XRD patterns of spray dried granules; (a) YZ-W, (b) YZ-AH and (c) YZ-AS.

to the study of developing microstructures in TBC layers by APS coating. Three sets of granules with a similar size (40-50 μm), but different morphologies were atomized through a fine nozzle and sprayed into a heated chamber. The granules were each fabricated under optimum conditions to produce different sizes and morphologies. It is known that the sprayed granules create a relatively inexpensive, free flowing, and appropriate porous microstructures to insulate high thermal environments effectively [9-11].

Fig. 3 shows XRD patterns that were measured on the spray dried granules from the water based solution, YZ-W, (Fig. 3(a)) and alcohol based solution, YZ-AH and YZ-AS (Fig. 3(b) and (c)). Tetragonal/cubic ZrO_2 peaks were observed with minor monoclinic peaks except YZ-AH.

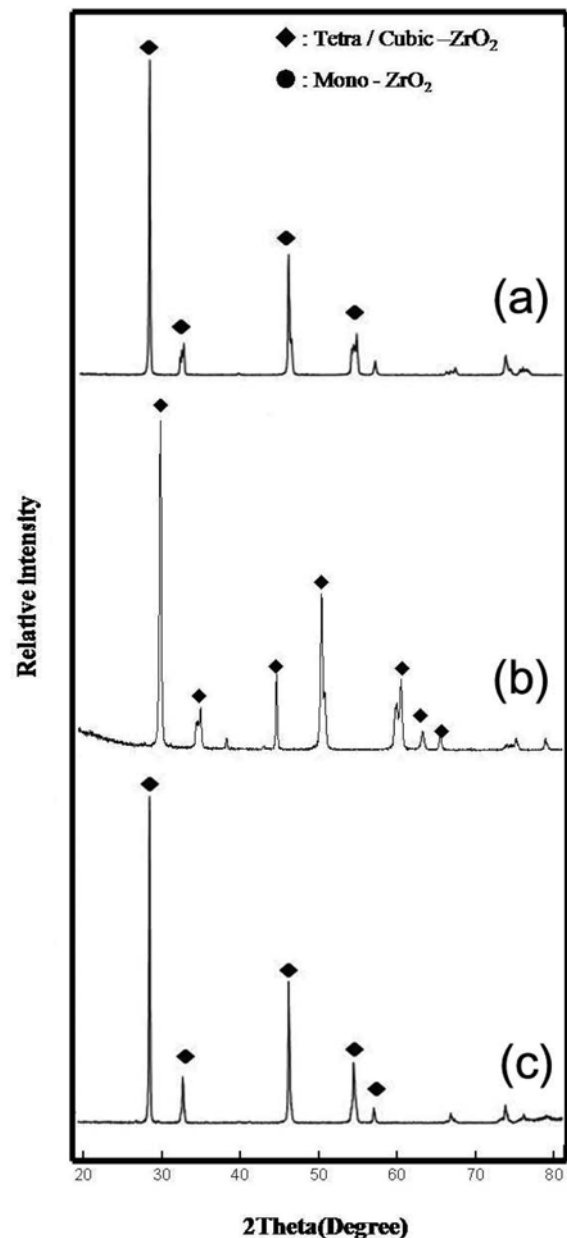


Fig. 4. XRD patterns of spray dried granules after heat treatment at 1250 $^{\circ}\text{C}$ for 10 min; (a) YZ-W, (b) YZ-AH and (c) YZ-AS.

XRD patterns that were measured after the heat treatments at 1250 $^{\circ}\text{C}$ for 10 minutes are shown in Fig. 4. We could not observe the monoclinic peaks after the heat treatments, indicating the significance of post heat treatment of sprayed granules. As the monoclinic phase is known to transform to the tetragonal and precipitates cubic phase that renders the tetragonal to monoclinic, in turn as the phase transformation may cause cracks and defects therefore it is necessary to remove the monoclinic phase.

The bar chart in Fig. 5 shows the feed rate for the three sets of spray dried granules. The feed rate is a critical parameter in the ability of the flow of granules during TBCs formation by APS. The feed rate improves strongly through the sequence YZ-W, YZ-AH and YZ-AS,

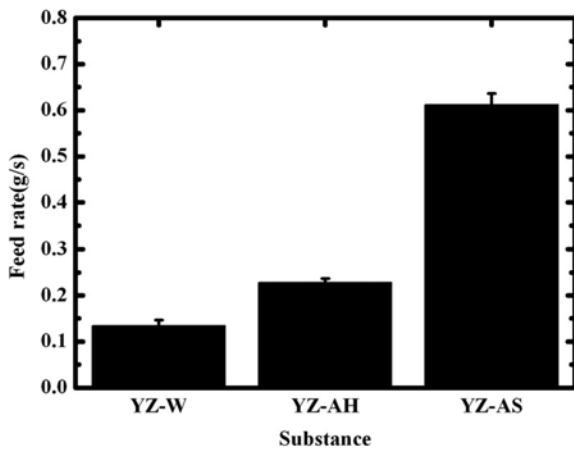


Fig. 5. The results of feed rate measurement of spray dried granules for YZ-W, YZ-AH and YZ-AS.

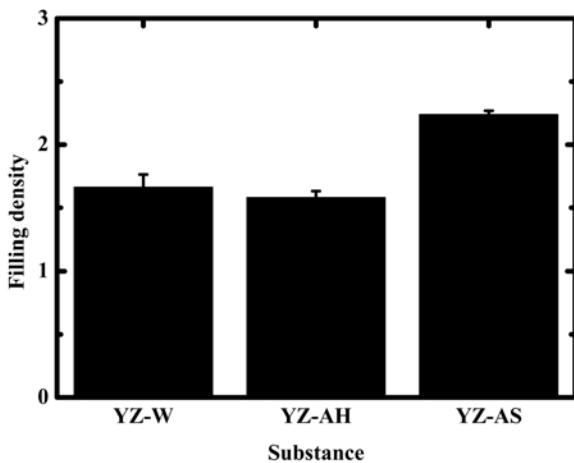


Fig. 6. The results of filling density measurements of spray dried granules for YZ-W, YZ-AH and YZ-AS.

commensurate with the powder morphology trend in Fig. 2. Fig. 6 shows the results of measured filling densities of YZ-W, YZ-AH and YZ-AS granules. Compared to YZ-W and YZ-AH, YZ-AS shows higher filling densities. Based on the results of Fig. 5 and Fig. 6, the degree of globular shape has an advantage of improving the feed rate and filling density in this study. The role of the spray dried morphology in the microstructure of the TBC layers has already been studied in the literature [11], but the links among the morphology, feed rate and thermal resistance have not been investigated. Some literature comments that if the powder is fine and porous, it cannot be fed into the center of the plasma flame or be evaporated before splatting on the substrate, resulting in a poor deposit efficiency and weak interfacial strength [9].

Experimental data for the measured thickness of TBC layers deposited using YZ-W, YZ-AH and YZ-AS granules, as a function of specimen position, are plotted in Fig. 7. The measured results show that the values are relatively unchanged for all TBC sections indicating the coating thickness is uniform in the TBC layer. A uniform TBC

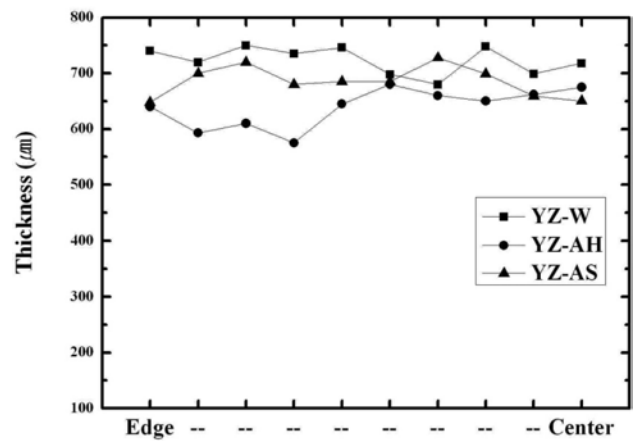


Fig. 7. The results of thickness measurement of TBC topcoat layers for YZ-W, YZ-AH and YZ-AS.

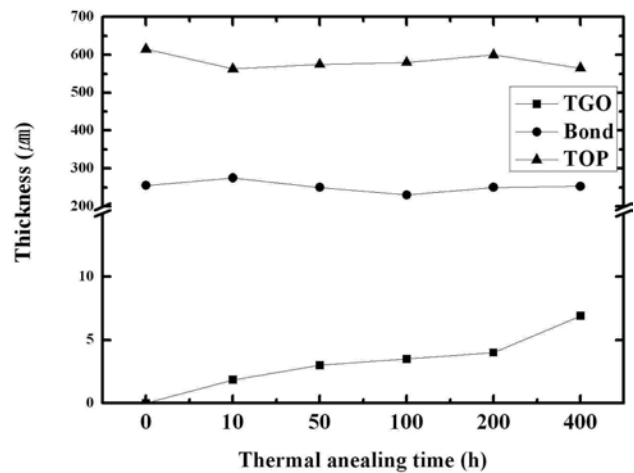


Fig. 8. Thickness variations of TBC topcoat deposited using YZ-W granules, bondcoat and TGO as a function of thermal annealing time at 1210 °C. Note the increase tendency for the TGO layer.

coating thickness could be obtained using the spray dried granules prepared in this study by an APS coating method. This result indicates an application of spray dried granules offers the development of TBCs successfully, and as the granules have a generally spherical shape, it is thought that the granules could be uniformly fed by the plasma gun and free flowing.

The TGO thickness measured by SEM at the interface between the top coat and the bond coat is shown in Fig. 8 as a function of thermal annealing time. The measurements were conducted for TBC layers deposited using YZ-W granules. The thicknesses of the TBC layers and the bondcoat layer were also measured and included in the graph. While the thickness of the TBC and the bondcoat layer are unchanged, the variation of the TGO thickness is clear in the graph. The TGO thickness tends to increase with an increase in the annealing time at high temperature, with a TGO thickness of 1.88 μm after 10 h annealing at 1210 °C and about 5 μm after 400 h annealing. I. T. Spitsberg and coworker [2] revealed that the TGO thickness is proportional to annealing time, $t^{1/2}$. Our result is in agreement with this model.

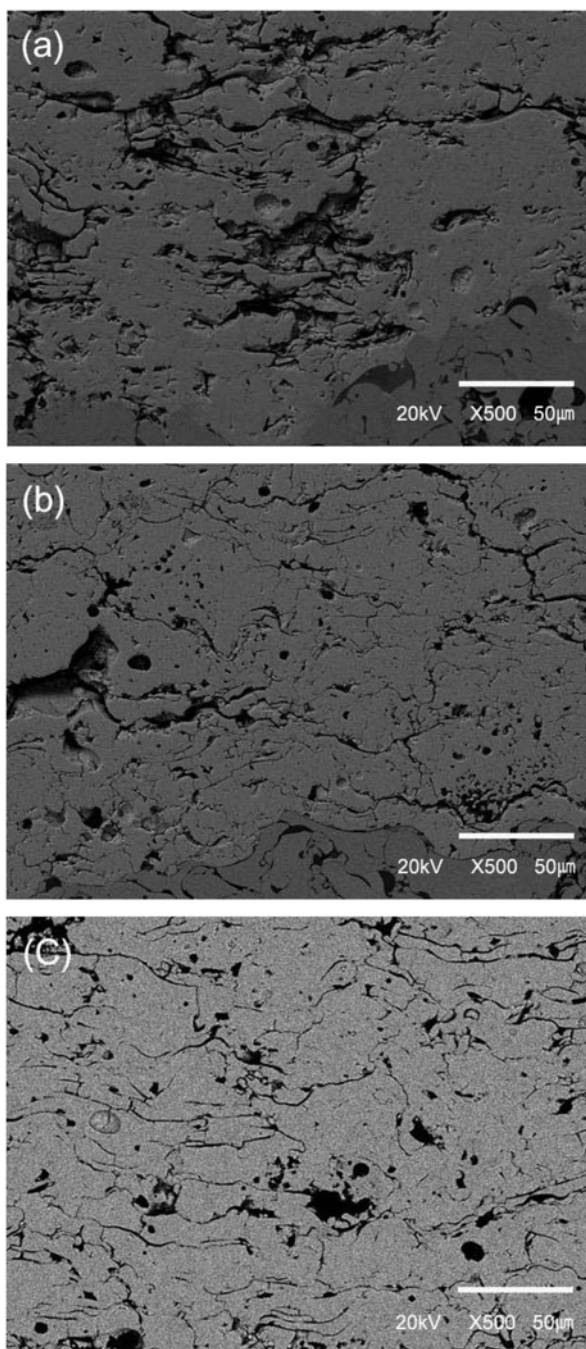


Fig. 9. SEM cross-section views of the TBC layers deposited using (a) **YZ-W** as-sprayed, (b) **YZ-AH** as-sprayed and (c) **YZ-W** after heat treatment at 1250 °C for 10 minute.

Optical micrographs showing TBC microstructures of sectioned surfaces after mechanical polishing are shown in Fig. 9. The microstructures include many pore volumes and splat boundaries. The dark circles in the polished TBCs sections are pores, and the irregular dark lines are splat boundaries in the micrographs. The microstructures of the TBC layers deposited using granules produced from a water-based solution (Fig. 9(a)), granules produced from an alcohol-based solution (Fig. 9(b)) indicate clear differences. While the TBC layers deposited using granules from a

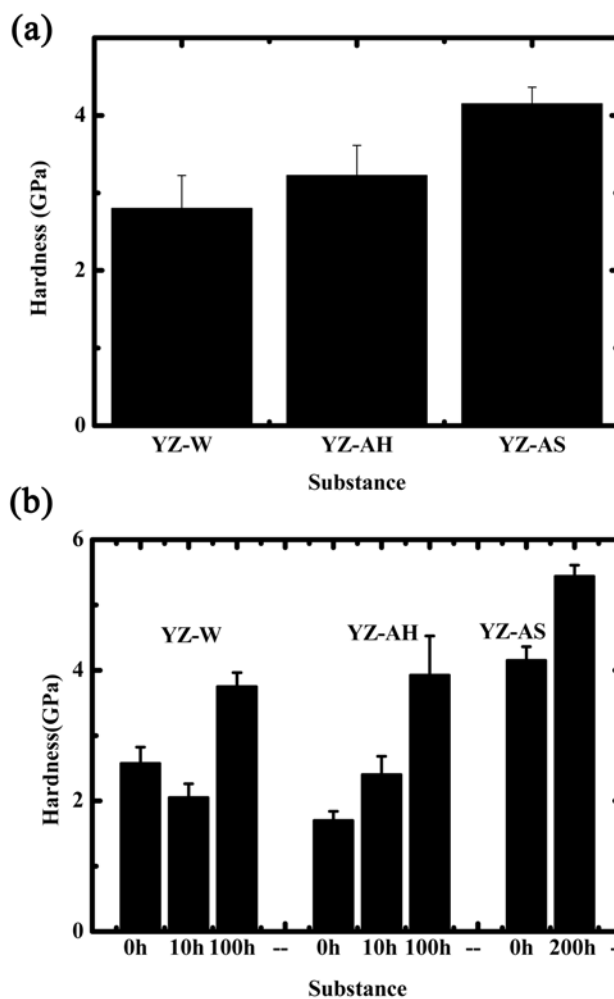


Fig. 10. The results of hardness measurements of TBC sections deposited using **YZ-W**, **YZ-AH** and **YZ-AS** (a) before thermal annealing and (b) after thermal annealing at 1210 °C for the time given.

water-based solution contains lots of defects of imperfect splat boundaries, the layers deposited from an alcohol-based solution contain smaller and uniform splat boundaries. Note the higher densities of splat boundaries in Fig. 9(b). On the other hand, we could change the irregular splat boundaries to uniform splat boundaries by heat treatment of the **YZ-W** granules as shown in Fig. 9(c). It seems possible that the heat treatment offers strength and fluidity of the granules during feeding into the substrate. The results in Fig. 9 indicate that the powder morphology is essential to the TBC microstructure.

Hardness, H of the TBC system measured using a Vickers indenter for TBC layers deposited using different morphologies of spray dried granules are shown in Fig. 10(a). It is noteworthy that the hardness increased through the sequence **YZ-W**, **YZ-AH** and **YZ-AS**, commensurate with the powder morphology trend in Fig. 2 and the sectioned views of the microstructures in Fig. 9. The hardness change after thermal fatigue for a constant time at 1210 °C for TBCs are plotted in Fig. 10(b). The fact that the values of H in the TBC are enhanced indicates that sintering

of the topcoat has been occurred. As the sintering of the topcoat causes defects or cracks, the thermal annealing caused interfacial delamination after 100 h holding for the TBC deposited using **YZ-W**. However, interfacial delamination in the TBCs deposited using **YZ-AH** and **YZ-AS** did not occur under the same conditions. Therefore it can be concluded that spherical spray dried granules prepared from an alcohol-based solution are candidate materials with high stability for TBC materials.

Conclusions

In this study yttria stabilized zirconia powders were synthesized using a co-precipitation method, and transformed to micrometre-sized granules by controlling the solvent type, binder/dispersant content and process parameters during spray process. We compared three types of powder morphologies: (i) deformed (ii) partially spherical and (iii) spherical. The spray dried granules were deposited over a NiCrCoAlY bond coat by an air plasma spray coating apparatus to form ceramic topcoat thermal barrier coatings. We evaluated the thermal resistance of the thermal barrier layers by thermal annealing tests and hardness measurements after the thermal annealing tests. As a result, the thermal barrier coating using pre-heat treated spherical powder gave advantages of thermal and mechanical tolerance after thermal annealing tests.

Acknowledgments

This work was supported by research program 2008 Kookmin University, MOCIE through EIRC, and the Seoul research and Business Development Program (Grant No. 10583).

References

1. D. Zhu and R.A. Miller, *Mater. Sci. Eng. A*, A245 (1998) 212-223.
2. I.T. Spitsberg, D.R. Mumm and A.G. Evans, *Mater. Sci. Eng. A*, A394 (2005) 176-191.
3. J.R. Nicholls, *MRS Bulletin Sep.* (2003) 659-670.
4. X.Q. Cao, R. Vassen and D. Stöver, *J. European Ceram. Soc.* 24 (2004) 1-10.
5. R.A. Miller, *Surf. Coat. Technol.* 30 (1987) 1-11.
6. M. Friis, C. Persson and J. Wigren, *Surf. Coat. Technol.* 141 (2001) 115-127.
7. H. Boukari, A.J. Allen, G.G. Long, J. Ilavsky, J.S. Wallace, C.C. Berndt and H. Herman, *J. Mater. Res.* 18 (2003) 624-634.
8. G. Bertrand, P. Bertrand, P. Roy, C. Rio and R. Mevrel, *Surf. Coat. Technol.* 202 (2008) 1994-2001.
9. X.Q. Cao, R. Vassen, S. Schwartz, W. Jungen, F. Tietz and D. Stöver, *J. Eur. Ceram. Soc.* 20 (2000) 2433-2439.
10. J.F. Li, H. Liao, X.Y. Wang, C. Coddet, H. Chen and C.X. Ding, *Thin Solid Films* 460 (2004) 101-115.
11. P. Roy, G. Bertrand and C. Coddet, *Powder Technol.* 157 (2005) 20-26.
12. D. Schwingel, R. Taylor, T. Haubold, J. Wigren and C. Gualco, *Surf. Coat. Technol.* 1-3 (1998) 99-106.
13. D. Zhu and R.A. Miller, *Surf. Coat. Technol.* 108-109 (1998) 114-120.
14. D. Zhu and R. A. Miller, *Surf. Coat. Technol.* 94-95 (1997) 94-101.
15. D. Zhu and R. A. Miller, *Mater. Sci. Eng. A*, A245 (1998) 212-223.
16. A.G. Evans, d. R. Mumm, J.W. Hutchinson, G.H. Meier and F.S. Pettit, *Progr. Mater. Sci.* 46 (2001) 505-533.
17. A.G. Evans and J.W. Hutchinson, *Surf. Coat. Tech.* 201 (2007) 7905-7916.